JGR Biogeosciences

RESEARCH ARTICLE
10.1029/2022JG006864

Key Points:

- Discontinuous permafrost environments are characterized by strong spatial heterogeneity and complex feedback loops
- Near-surface hydrology and soil properties are strong drivers of spatial heterogeneity in these systems
- Missing representation of subgrid heterogeneity in Terrestrial Ecosystem Models could bias predictions of high-latitude carbon budget

Supporting Information:

Supporting Information may be found in the online version of this article.

Correspondence to:

I. A. Shirley,
IShirley@lbl.gov

Citation:

Shirley, I. A., Mekonnen, Z. A., Wainwright, H., Romanovsky, V. E., Grant, R. F., Hubbard, S. S., et al. (2022). Near-surface hydrology and soil properties drive heterogeneity in permafrost distribution, vegetation dynamics, and carbon cycling in a Sub-Arctic watershed. *Journal of Geophysical Research: Biogeosciences*, *127*, e2022JG006864. https://doi.org/10.1029/2022JG006864

Received 16 FEB 2022
Accepted 30 JUN 2022

Near-Surface Hydrology and Soil Properties Drive Heterogeneity in Permafrost Distribution, Vegetation Dynamics, and Carbon Cycling in a Sub-Arctic Watershed

Ian A. Shirley[1,2], Zelalem A. Mekonnen[1], Haruko Wainwright[1], Vladimir E. Romanovsky[3], Robert F. Grant[4], Susan S. Hubbard[1], William J. Riley[1], and Baptiste Dafflon[1]

[1]Earth and Environmental Sciences Area, Lawrence Berkeley National Laboratory, Berkeley, CA, USA, [2]Department of Physics, University of California-Berkeley, Berkeley, CA, USA, [3]Geophysical Institute, University of Alaska Fairbanks, Fairbanks, AK, USA, [4]Department of Renewable Resources, University of Alberta, Edmonton, AB, Canada

Abstract Discontinuous permafrost environments exhibit strong spatial heterogeneity at scales too small to be driven by weather forcing or captured by Earth System Models. Here we analyze effects of observed spatial heterogeneity in soil and vegetation properties, hydrology, and thermal dynamics on ecosystem carbon dynamics in a watershed on the Seward Peninsula in Alaska. We apply a Morris global sensitivity analysis to a process-rich, successfully tested terrestrial ecosystem model (TEM), *ecosys*, varying soil properties, boundary conditions, and weather forcing. We show that landscape heterogeneity strongly impacts soil temperatures and vegetation composition. Snow depth, O-horizon thickness, and near-surface water content, which vary at scales of O(m), control the soil thermal regime more than an air temperature gradient corresponding to a 140 km north–south distance. High shrub productivity is simulated only in talik (perennially unfrozen) soils with high nitrogen availability. Through these effects on plant and permafrost dynamics, landscape heterogeneity impacts ecosystem productivity. Simulations with near-surface taliks have higher microbial respiration (by 78.0 gC m^{-2} yr^{-1}) and higher net primary productivity (by 104.9 gC m^{-2} yr^{-1}) compared to runs with near-surface permafrost, and simulations with high shrub productivity have outlying values of net carbon uptake. We explored the prediction uncertainty associated with ignoring observed landscape heterogeneity, and found that watershed net carbon uptake is 60% larger when heterogeneity is accounted for. Our results highlight the complexity inherent in discontinuous permafrost environments and demonstrate that missing representation of subgrid heterogeneity in TEMs could bias predictions of high-latitude carbon budget.

Plain Language Summary At high-latitudes, properties such as soil temperatures, soil wetness, snowpack, and vegetation cover vary considerably across a landscape. The scale of this variation can be as small as 1–10 m (e.g., a patch of tall shrubs with a deep snowpack and warm soil temperatures is surrounded by low-lying tundra vegetation with shallow snowpack and cold soil temperatures). The resolution of terrestrial ecosystem models that are used to predict global responses to climate change, however, is much coarser (~100–300 km). The mismatch between the scales of landscape variation and the scales of models may introduce bias into predictions of ecosystem processes. In order to better understand the causes and implications of landscape variability, we explore the response of an ecosystem model to variation in soil properties, boundary conditions, and weather forcing. We find that landscape variability in snowpack and soil properties strongly influences soil temperatures, vegetation cover, and ecosystem carbon cycling. In particular, we show that net carbon uptake of the studied area is 60% higher when we account for the observed variability in shrub distribution. These results demonstrate the need for higher resolution measurements and improved model representation of landscape variability.

1. Introduction

High-latitude ecosystems are integral to the global carbon cycle, in part because of the large carbon stocks stored in permafrost soils (Rogelj et al., 2019; Schuur et al., 2015). However, spatial heterogeneity in permafrost ecosystems drives uncertainty in predictions of carbon cycle responses to climate change (Lara et al., 2020; Treat et al., 2018). The horizontal grid spacings of CMIP5 and CMIP6 models used by the IPCC to forecast the global response to climate change (~100–300 km; Strandberg & Lind, 2021) are much coarser than typical scales of

landscape heterogeneity in permafrost ecosystems. In these systems, snow depth, soil properties, and vegetation composition can vary over horizontal distances of 1–10 m (Grant, Mekonnen, Riley, Wainwright, et al., 2017; Uhlemann et al., 2021)

Landscape heterogeneity is particularly pronounced in discontinuous permafrost environments, where perennially frozen (permafrost) and perennially unfrozen (talik) soils coexist at local scales (~O(m); Uhlemann et al., 2021; Zoltai, 1993). Such strong heterogeneity in subsurface physical conditions is created by complex interactions and feedbacks between climate, hydrology, soil properties, and vegetation (Jorgenson et al., 2010). Local variation in snow depth is a primary driver of soil temperature heterogeneity across the arctic (Jafarov et al., 2018; O'Neill & Burn, 2017; Taras et al., 2002b). Feedback loops are important in these systems, as some controls on high-latitude soil temperatures, such as soil organic matter content (D. Zhu et al., 2019) and vegetation cover (Debolskiy et al., 2020; Jafarov et al., 2018; Park et al., 2018), respond to heterogeneity in soil temperatures via changes in microbial activity (Waldrop et al., 2021) and vegetation dynamics (Becker et al., 2016; Jafarov et al., 2018; Mekonnen, Riley, Grant, et al., 2021). Soil thermal state also has a strong impact on nitrogen availability (Finger et al., 2016; Keuper et al., 2012) and carbon fluxes (Belshe et al., 2012; Nobrega & Grogan, 2008) at high latitudes.

While many relationships between environmental factors and spatial variability in soil temperature, vegetation dynamics, and carbon fluxes have been identified, system complexity complicates field and modeling efforts to characterize the relative importance of each driver in producing local heterogeneity (Arora et al., 2019). Further, these environmental factors operate in the context of the local climate, and quantification of the strength of each driver relative to variability in regional climate controls, while important, is an added challenge. Landscape heterogeneity is a characteristic feature of ecosystems across the globe and efforts have been made to characterize and represent the impacts of heterogeneity in vegetation cover (Cable et al., 2016), hillslope position (Mekonnen, Riley, Grant, et al., 2021), and microtopography (Grant, Mekonnen, Riley, Arora, et al., 2017) on soil temperatures, vegetation, and carbon fluxes. Nevertheless, the level of detail in representation of sub-grid heterogeneity needed to accurately represent key system processes in TEMs remains unclear. In particular, more work is needed to understand how missing model representation of landscape heterogeneity (e.g., snow depths, landscape position, soil thermal and hydrologic condition, and vegetation cover) in a TEM grid-cell impacts representation of carbon cycle dynamics in discontinuous permafrost ecosystems.

In this study, we explore how variability in soil properties, landscape position, and weather forcing affect variability in soil thermal regimes, vegetation dynamics, and carbon cycling as simulated in a one-dimensional TEM. We perform a global sensitivity analysis (GSA) using *ecosys*, a TEM that has been well-tested at high-latitudes (see reviews of model performance in Mekonnen, Riley, Grant, et al., 2021; Mekonnen, Riley, Randerson, et al., 2019; Riley et al., 2021; Shirley, Mekonnen, et al., 2022), varying soil properties, boundary conditions, and weather forcings over ranges that represent the variability found in a watershed on the Seward Peninsula in Alaska. Because of the computational demands, process richness, and nonlinearity of this model, we use the Morris one at a time method, a difference based GSA with computational costs that scale linearly with the number of factors explored (Morris, 1991; Wainwright et al., 2014). We first show that the simulations generated in the GSA cover the range of soil temperatures, water contents, and surface CO_2 fluxes observed within the watershed. Then, we use the GSA results to identify and rank the drivers of variation in soil temperatures, permafrost distribution, and vegetation composition. Finally, we explain how this variation impacts ecosystem productivity and explore the prediction uncertainty associated with ignoring observed landscape heterogeneity.

2. Methods

2.1. The *Ecosys* Model

Ecosys has been applied in many published studies of high-latitude ecosystems, and has been shown to accurately represent thermal and hydrological dynamics (Grant, Mekonnen, and Riley, 2019; Grant, Mekonnen, Riley, Wainwright, et al., 2017), plant processes (Mekonnen, Riley, Grant, et al., 2021; Mekonnen, Riley, Randerson, et al., 2019), and soil microbial activity and carbon fluxes (Grant, Mekonnen, and Riley, 2019; Grant, Mekonnen, Riley, et al., 2019; Grant, Mekonnen, Riley, Wainwright, et al., 2017). We have included a detailed description of ecosys performance in high-latitude systems in the SI. Below, we give a brief description of model processes related to soil thermal dynamics, carbon cycling, and PFT dynamics. A comprehensive description of *ecosys* is given in the Supplementary Material of Mekonnen, Riley, Randerson, et al. (2019).

Ecosys is an hourly time-step ecosystem model with tightly coupled energy, water, nutrient, and C cycles. The model is forced with hourly meteorological inputs and represents a multi-layer canopy, a litter residue layer, a multi-layer soil column, and a seasonal snowpack. Canopy energy balance is calculated using first-order closure schemes by forcing the sum of net radiation, latent heat, sensible heat, and soil heat to zero. Heat is exchanged between the canopy and the residue layer or snowpack, and is then transferred through the soil column via conduction and advection. The thermal properties of each soil layer are determined by organic and mineral components, soil bulk density, water content, and temperature. Application of the general heat flux equation causes soil freezing (thawing) to begin when the temperature of a soil layer falls below (rises above) a freezing point that is calculated using the soil layer water potential.

Water influx via precipitation, snow melt or water table exchanges is transferred with associated concentive heat through soil and root profiles. In soil micropores, water transfer between adjacent layers is calculated using Richard's equation if the layers are either both saturated or unsaturated. If a wetting front exists, the Green-Ampt equation is used. In soil macropores, water flow is simulated using Poiseuille–Hagen theory for laminar flow in tubes. Root water flow is driven by transpiration from dry surfaces and evaporation from wet surfaces in vascular and non-vascular plants. Evapotranspiration is driven by to canopy energy exchange, and depends on soil, root, and canopy water potentials and root hydraulic resistances (Mezbahuddin et al., 2016).

In the version of *ecosys* used here, snowpack is modeled as a single uniform layer that contains snow, water, ice and gas. The density depends on snowpack thickness and on snow, ice, and water contents. Snowpack thermal conductivity is calculated using snowpack density, and heat capacity is calculated using snow, ice, and water contents. Phase changes within the snowpack can occur via precipitation inputs, melting, evaporation, and sublimation.

The model is seeded with plant functional types (PFTs) that are common to the studied region (deciduous broadleaf shrub, moss, lichen, grass, and sedge). The relative dominance of each PFT is emergent in the model in response to competition for light, water, and nutrients. Different strategies for canopy and root growth, water use, and nutrient acquisition and retention are represented by PFT-specific functional traits for CO_2 fixation kinetics, leaf optical properties, phenology, morphology, nutrient recycling, and root traits.

Canopy CO_2 fixation is determined by availability of CO_2, light, water, and nutrients. Within each leaf, carboxylation is calculated using light and CO_2 availability according to the Farquhar biogeochemical growth model (Farquhar et al., 1980). Stomatal conductance maintains internal to ambient CO_2 ratio unless conductance is reduced by low canopy turgor (Grant & Flanagan, 2007). Oxidation of photosynthesized sugars is first used to fulfill maintenance respiration needs. Excess sugars are stored in non-structural C pools or oxidized to drive shoot and root growth and active nutrient uptake.

Mobilization of carbon and nutrient pools is directed into growth of vertical primary roots and lateral secondary roots according to PFT-dependent root radii and branching densities. Plant nutrient uptake is coupled with nutrient diffusion and advection from the soil solution to root surfaces. Soil solution nutrient concentrations are governed by nutrient mineralization or immobilization rates driven by microbial biomass stoichiometry. Inhibition of plant nutrient uptake is determined by stoichiometry of stored pools of carbon and nutrients (Grant, 1998).

Microbial growth is driven by oxidation of dissolved organic carbon substrates. Oxidation rates are controlled by substrate concentration, soil temperature, soil water content, and availability of oxygen and nutrients. Dissolved organic carbon is produced via microbially driven hydrolysis of soil organic matter consisting of woody litter, non-woody litter, particulate organic matter, humus, microbial biomass each with components that have different susceptibilities to hydrolysis (Grant, 2014).

2.2. Morris Sensitivity Analysis

The Morris Method is a one-factor-at-a-time sensitivity analysis designed to cover large factor spaces efficiently (Wainwright et al., 2014; Morris, 1991). The Morris Method is a GSA, meaning that it is robust to non-linearity and interaction effects among factors. In this method, each factor is allowed to vary within a prescribed range that defines the factor space to be explored. The factor space is not continuous, however, since each factor can only take p discrete values that are equally distributed throughout the prescribed range. Trajectories or paths of runs are generated, where each of the k factors is changed by a fixed increment Δ from a randomly selected

initial value, where Δ represents $p/(2(p-1))$ times the factor range. The order in which the factors change is also randomly generated, and the process is repeated r times (Morris, 1991). An approach pioneered by Campolongo et al. (2007) and improved by Ruano et al. (2012) to generate sets of trajectories that optimally cover the factor space is used in this work.

In a Morris sensitivity analysis, the metric used to characterize the influence of a factor x on an output y is called the elementary effect (EE). The EE of x on y is defined as the difference in the output y between two neighboring runs (where only one factor, x, has been changed) divided by Δ. The EE of a factor on an output can be interpreted as the change in the output that would be expected when the factor is changed from the minimum value to the maximum value in its range. Since there are r trajectories, the EE for each x and y can be calculated r times. Typically, the mean EE, the mean of the absolute value of the EE, and the standard deviation of the EE are calculated. Since the mean absolute EE is insensitive to the sign of each EE, this metric characterizes the relative importance of each factor on each output. If the mean absolute EE of a factor on an output is large, a change in the factor leads to a large change in the output. The mean EE gives information on the sign of the effect. If the mean EE of a factor on an output is negative, then an increase of the factor leads to a decrease of the output on average. Non-linearities or interaction effects can be identified by plotting the EE as a function of the factor value and/or by comparing the magnitude of the mean EE with the mean absolute EE. When the mean EE is smaller than the mean absolute EE, the sign of the EE changes depending on the location in factor space. The impact of a factor on a model output is considered to be significant if the mean EE or mean absolute EE are larger than two times standard error of the EE, as in Morris (1991).

2.3. Site Data and Meteorological Forcing

This study is undertaken as part of the Next-Generation Ecosystem Experiment (NGEE-Arctic project). The NGEE-Arctic project aims at improving Earth System models through interdisciplinary and coordinated investigation of arctic terrestrial ecosystems. In this work, we focus on a watershed within the Seward Peninsula that has been the subject of extensive investigation by the NGEE Arctic project (Léger et al., 2019; Uhlemann et al., 2021).

The studied watershed is located about 40 km northwest of Nome along Teller road and occupies an area of approximately 2.3 km^2. The topography of the watershed is characterized by a 130 m elevation gradient that leads to the emergence of heterogeneous properties. Solifluction lobes, drainage paths, and other meter-scale microtopographic features generated by variable permafrost degradation are found throughout the watershed. At some locations, the permafrost table is close to the surface, at 0.5 m or shallower, and at others there is a talik below the active layer and the permafrost table is deep or absent. Across the watershed, bedrock depth likely varies from meters to tens of meters, O-horizon thickness varies from a few centimeters to tens of centimeters, and mixtures of low-lying tundra vegetation (dwarf shrubs, bryophytes, graminoids, and sedges) are interspersed with patches of deciduous willow shrubs (*Salix* spp) reaching heights of 3 m.

Nine intensive monitoring stations are distributed around the watershed, each with soil temperature at 2, 25, 50, 100, and 150 cm depths and volumetric water content (VWC) sensors at 10, 25, and 50 cm depths (V. Romanovsky et al., 2020). At 1.5 m depth, measured peak soil temperatures at these sites vary by more than 5°C (from −0.2°C to 5.7°C). While some sites never rise above 0°C at 1.5 m depth for the years 2016–2018, others never freeze at depths much closer to the surface (Figure 1). In 2017, 2018, and 2019, snowpack thickness was measured across the watershed in the spring before the onset of snowmelt. In 2019, a high snow year, snow depths measured across the watershed on April 1 (near peak snowpack) ranged from 14 to 214 cm. At six sites characterized by distinct vegetation cover and soil saturation in a small subset of the studied watershed, we deployed *Eosense FD* chambers to measure soil CO_2 fluxes throughout the 2019 growing season and into the fall. At these sites, peak daily mean CO_2 flux ranged from 1 μmol m^{-2} s^{-1} to greater than 5 μmol m^{-2} s^{-1} and the date that soil CO_2 flux dropped below 0.5 μmol m^{-2} s^{-1} ranged from early August to mid November.

The GSA *ecosys* simulations were run from 1836 to 2019 at hourly temporal resolution. Each GSA simulation was spun up independently. For the years 1836–1979, values for air temperature at 2 m, incoming shortwave radiation, precipitation, wind speed at 10 m, and relative humidity at 2 m were taken from the NOAA-CIRES-DOE twentieth Century Reanalysis V3 product (Slivinski et al., 2021). For the years 1980–2019, values for air temperature at 2 m, wind speed at 10 m, and relative humidity at 2 m were taken from the North American

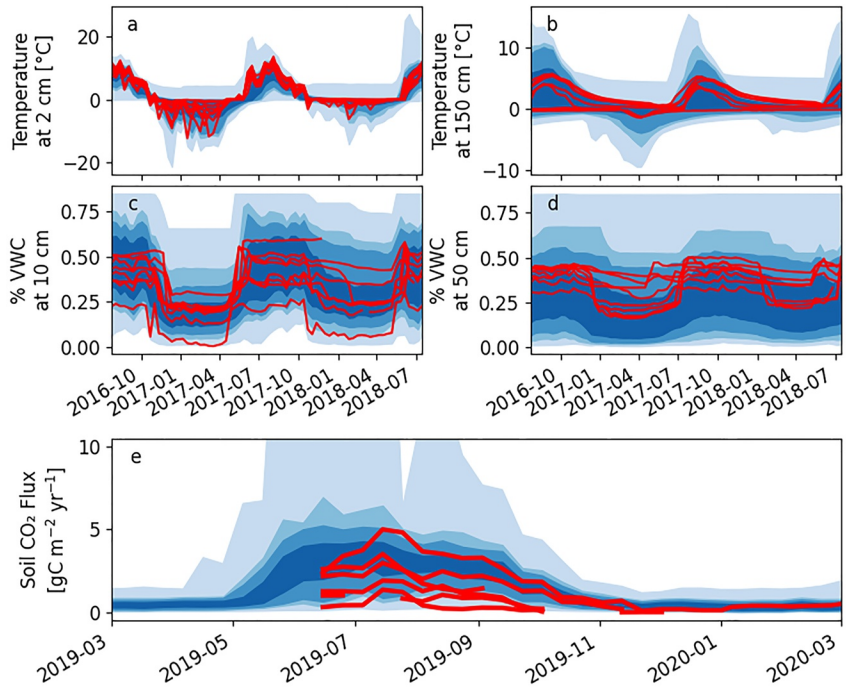

Figure 1. Site soil conditions are represented in the sensitivity analysis runs. Monitoring data (red lines) is shown for soil temperature for the shallowest (a) 2 cm and deepest measurement (b) 150 cm and soil volumetric water content (volumetric water content %VWC) for the shallowest (c) 10 cm and deepest (d) 50 cm measurement at seven distinct ecotypes distributed across the watershed between August 2016 and August 2018. Observed at six locations (red lines) and ensemble modeled (blue) soil CO_2 fluxes (e) for the 2019 growing season and into the fall. Distributions for the sensitivity analysis model outputs for each variable are shown blue (blue shades from light to dark represent the 0–100th, 5–95th, 10–90th, and 25–75th percentile ranges, respectively).

Regional Reanalysis (NARR; Wei et al., 2014), and values for incoming shortwave radiation and precipitation were taken from the Modern-Era Retrospective Analysis for Research and Applications, version 2 (MERRA-2; Gelaro et al., 2017). Data from two weather stations located at the top and near the bottom of the watershed (Busey et al., 2017) for the years 2017–2019 were used to bias correct these weather products. Atmospheric CO_2 concentrations were increased according to historic concentrations for years 1836–2019, and the rate of atmospheric N deposition for the site was taken from Dentener (2006).

2.4. Sensitivity Analysis Design

Here, we run a Morris sensitivity analysis of the *ecosys* model to changes in 24 factors related to soil properties, boundary conditions, and weather forcings. The range chosen for each factor is meant to capture the possible range of values that might be observed within a 100 km radius of the studied watershed. Some of these ranges are chosen to create differences in our 1D simulations consistent with differences expected from landscape position in a fully 3D model (e.g., snow interactions with microtopography and vegetation, water table interactions with hillslope position, radiation interactions with aspect). Each factor in the analysis can take 6 discrete and evenly distributed values within the prescribed range (Table 1).

The simulated soil column is 40 m thick with 20 layers that are grouped into three types (O-horizon, A/B horizon, bedrock). The thickness and other properties of each soil type are modified independently. The O-horizon has high organic matter content (50%–100% by weight) and a variable thickness of 0–40 cm. Water retention and drainage in organic soils are highly variable. Hemic and sapric peat soils have high water retention, but fibric peat soils, which have large macropore fractions, are typically well drained (Dimitrov et al., 2010). We represent this in the GSA by varying the macroporosity of the O-horizon from 50% to 100% by volume. The A/B horizon is primarily mineral soil that extends from the bottom of the O-horizon to the top of the bedrock. The organic matter content of this layer ranges from 0.5% to 20% by weight. Sand content of this layer can range from 0% to

Table 1
Factor Description for the Morris Global Sensitivity Analysis

Name	Description	Units	Min	Max
OH thickness	O-horizon thickness	m	0	0.40
BR depth	Soil layer of top of bedrock	na	10	20
OH MP	Macroporosity of the O-horizon	%	0	50
A/B MP	Macroporosity of the A/B horizon	%	0	15
BR MP	Macroporosity of the bedrock	%	0	15
A/BH rock	A/B-horizon rock content	%	0	15
OH OM	O-horizon organic matter content	gC kg^{-1}	500	1,000
A/BH OM	A/B-horizon organic matter content	gC kg^{-1}	5	200
A/BH Sand	A/B-horizon sand content	g kg^{-1}	0	1,000
A/BH Clay	A/B-horizon clay content	g kg^{-1}	0	200
pH	pH of soil profile	na	4.5	8
C:N	C:N of soil profile	na	10	30
C:P	C:P of soil profile	na	50	300
Minerals	Exponential modifier of soil concentration of Ca, Mg, Na, Sulfate, and Cl	na	−3	2
Sulfate	Exponential modifier of soil concentration of sulfate	na	−3	3
Initial Ice	Initial soil ice content	% of porosity	0	95
Snow	Percent of prescribed snow precipitation	%	10	160
Rain	Percent of prescribed rain precipitation	%	66	133
Air T	Degrees added to prescribed air temperature	°C	−1	1
Wind	Percent of prescribed wind	%	50	200
SW In	Percent of prescribed Incoming SW radiation	%	75	125
Slope	Slope	na	0	25
MAT	Mean annual temperature at lower boundary	°C	−1	1
WT	Depth to external water table, sets lateral hydrological boundary conditions	m	0.2	3.2

Note. The name, description, units, and range of values is given for each factor that is varied in the GSA. Since ion concentrations can vary by many orders of magnitudes in arctic soils (Wu et al., 2018), Ca is varied from 10^{-3}–10^{2} mg/L, Mg is varied from 10^{-2}–10^{3} mg/L, Na is varied from 10^{-1}–10^{4} mg/L, K is varied from 10^{-3}–10^{2} mg/L, SO_x is varied from 10^{-3}–10^{3} mg/L, and Cl is varied from 10^{-1a}–10^{4} mg/L.

100% of the non-organic soil by weight, and clay content can range from 0% to 20% by weight, and the remaining mineral soil is silt. The impacts of gravelly soil on thermal properties and drainage are represented by the A/B-horizon rock and macroporosity, both of which can vary from 0% to 15% by volume. The bedrock is solid rock with fractures represented by variation in bedrock macroporosity from 0% to 15% by volume. In the GSA, depth to bedrock can take values of 0.8, 1.5, 2.5, 5, 15, or greater than 40 m. C:N, C:P, pH, and ion concentrations are modified throughout the soil profile. Changes in the lateral hydrological boundary conditions and the mean annual temperature of the bottom of the modeled soil column affect heat and water flux boundary conditions and thereby soil moisture and temperature.

In the GSA, we also modify site weather conditions. These modifiers remain constant throughout the entire 183 years simulation. Snow precipitation is varied from 10% to 160% of the prescribed value in order to represent the large variability in snow depths across the watershed created by wind redistribution of snow to microtopographic lows and areas of tall shrubs. Modeled maximum annual snow depths respond linearly to these changes in snow precipitation (Figure S1 in Supporting Information S1), so for simplicity we assume snow precipitation is a direct proxy for snow depth in the analysis below. Air temperature, rain, wind, and incoming shortwave radiation are modified to reflect measurement uncertainty and watershed-to regional-scale variations. For example, we vary mean annual air temperature over a 2°C range, which corresponds to a 140 km north-south distance at our site (NARR; Wei et al., 2014).

We calculate mean EEs and mean absolute EEs for mean soil temperatures (at the surface, 90 cm, and 275 cm), carbon fluxes (R_h, NPP, and NEE), and PFT mean annual NPP (shrub, moss, and sedge). To aid analysis of

interactions between soil thermal regimes, vegetation dynamics, and carbon cycling, we classify each GSA simulation using mean annual soil temperatures at 90 cm (90 cm MAT) for the years 2015–2019. In this classification, Talik runs have minimum annual temperatures greater than −0.1°C at 90 cm, shallow permafrost runs (shallow PF table) have maximum annual temperatures less than −0.1°C at 90 cm, and all other runs are classified as deep active layer runs (deep AL). Runs classified as deep AL may or may not be underlain by permafrost. The runs for each class are located in a different quadrant in the second row of Figure S2 in Supporting Information S1. We chose to perform this classification at 90 cm depth to balance relevance of biological processes and permafrost dynamics. At shallower depths, MATs exhibit large interannual variability and there are few runs with permafrost, whereas at deeper depths, soil thermal processes become largely disconnected with biological activity. MAT at a similar depth has been used in previous studies in the region to connect permafrost and vegetation dynamics (Cable et al., 2016).

3. Results and Discussion

3.1. GSA Outputs Reflect the Spatial Variability Observed in the Watershed

The system dynamics are spatially heterogeneous, depending on the different soil physical conditions, snow depths, and vegetation cover that can be found across the watershed. This spatial variability is well captured by the outputs of the GSA. In the GSA, the 10th (90th) percentile for peak soil temperatures at 1.5 m depth is −0.5°C (10°C). Throughout the years 2015–2019, soil temperatures at 30 cm never dropped below −0.1°C in 80 simulations and soil temperatures at 90 cm never rose above −0.1°C in 54 simulations. The 10th (90th) percentile snow depth on 1 April 2019 is 12 cm (196 cm), and the 10th (90th) percentile peak daily mean soil CO_2 flux for the year 2019 is 1.6 μmol m^{-2} s^{-1} (6.2 μmol m^{-2} s^{-1}). In general, the GSA outputs cover the range of soil temperatures, water contents, snow depth, and soil CO_2 fluxes observed in the studied watershed (Section 2.4; Figure 1).

In general, we do not expect distributions of soil physical conditions, snow depths, or carbon fluxes in the GSA to match the distributions of these variables in the watershed. The GSA is designed not to recreate the distributions of each weather forcing, soil property, and boundary condition in the watershed, but to quantify the effect of each factor across the entire space. It is likely, therefore, that some combinations of factors in the GSA simulate conditions that do not exist in the watershed. However, the GSA outputs cover the range of observed soil physical conditions, snow depths, or carbon fluxes and thereby provides important confirmation that the chosen ranges for each factor are appropriate for the site.

3.2. Near-Surface Hydrology and Soil Properties Drive Large Spatial Heterogeneity in Soil Temperatures

The Morris GSA employed in this study allows for quantitative comparison of the drivers of modeled soil temperatures. We find that local variation in near-surface hydrology and soil properties are the primary drivers of variation in soil temperature heterogeneity in the studied watershed. Specifically, snow depth, O-horizon macroporosity, external water table depth (which sets the lateral hydrological boundary conditions), and O-horizon thickness have similar or larger mean absolute EEs on 90 cm MAT than does a 2°C offset in air temperature (MAAT; Figures 2a and 2b). The EEs of each factor on MAT are very similar throughout the soil profile (Figure S3 in Supporting Information S1). At the surface, however, MAAT has a larger relative mean EE than deeper in the soil profile, and is ranked second only to snow depth. Most of the simulations in the GSA are classified as talik (Table S1 in Supporting Information S1). Consistent with the controls on soil temperature identified by the Morris GSA, permafrost is only modeled under conditions of shallow snowpack, high O-horizon macroporosity, and low air temperature (Figure S4 in Supporting Information S1).

In the GSA, snow depth has a larger impact on modeled soil temperatures than do any of the other factors, consistent with extensive literature documenting the strong influence of snow depth on soil and ground surface temperatures in the arctic (Jafarov et al., 2018; O'Neill & Burn, 2017; Taras et al., 2002a). For the years 2015–2019, the mean absolute EE of snow precipitation on 90 cm MAT is 3.3°C. This effect is twice as large as the mean absolute EE of the next most important factor. By providing strong insulation from cold winter air temperatures, snow creates an offset between MAAT and mean annual ground surface temperature (MAGST; Figures 2a and 2b), thereby warming soil temperatures. However, interactions between snow and soil temperatures are highly nonlinear and the soil warming effect of an increasing snowpack is much larger at lower snow depths. MAT at 90 cm

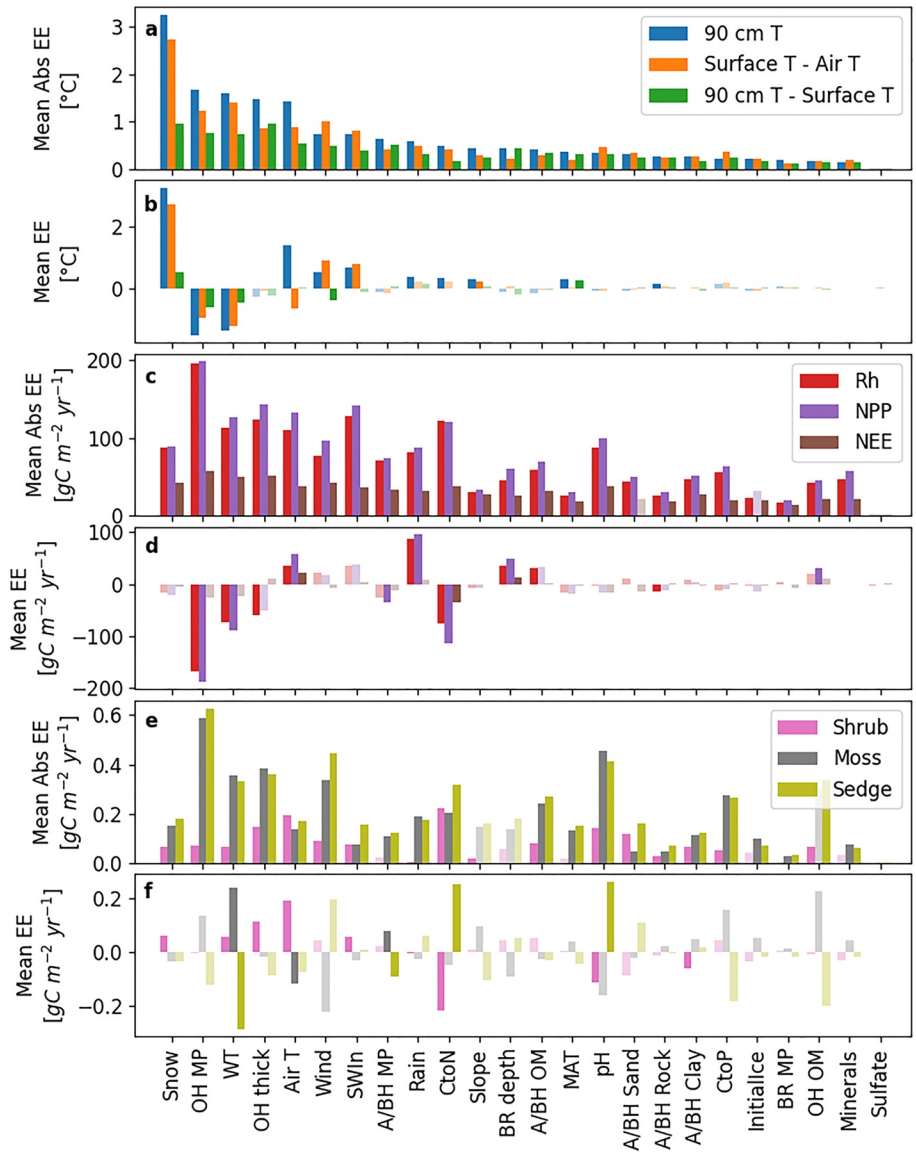

Figure 2. Sensitivity analysis showing controls for soil temperature, carbon fluxes, and plant functional type responses. Mean Elementary Effect (EE) and mean absolute EE for each factor are shown for mean annual soil temperature at 90 cm depth, difference between mean annual ground surface temperature and mean annual air temperature, and difference between mean annual soil temperature at 90 cm depth and mean annual ground surface temperature (a and b); mean annual R_h, NPP, and NEE (c and d); and relative dominance of shrub, moss, and sedge mean annual NPP (e and f) for the years 2015–2019. Significant factors for each variable and metric are shown in solid colors, non-significant factors are shown in semi-transparent colors. Following the methodology described in Morris (1991), a factor is determined to be significant if the mean EE or mean absolute EE are larger than two times the standard error of the EE. factor descriptions and ranges can be found in Table 1.

increases rapidly as snow precipitation approaches 70% of the prescribed value (corresponding to peak snow thickness of ~80 cm), but does not change much if more snow is added to the simulation (Figure 3).

O-horizon thickness is frequently cited as an important driver of permafrost distribution at high-latitudes, with thicker O-horizons associated with shallower active layer depths and colder soil temperatures due to the low thermal diffusivity of organic matter (D. Zhu et al., 2019; Johnson et al., 2013). Here, in contrast, O-horizon thickness EE can be either positive or negative due to interaction effects with other factors (Figure 3). The net result is a small and non-significant mean EE for O-horizon thickness on mean annual 90 cm depth soil T, even though the mean absolute EE of O-horizon thickness on 90 cm MAT is comparable to the mean absolute EE of air

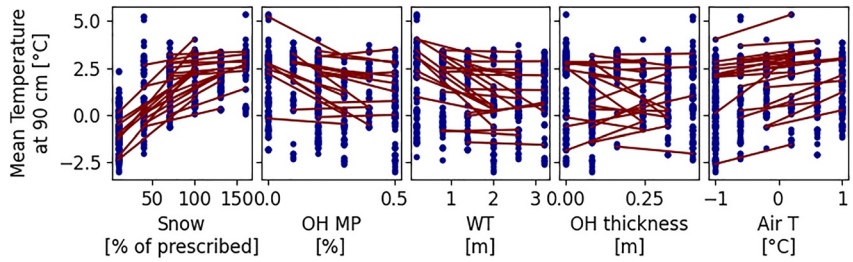

Figure 3. Responses of modeled soil temperature to factor changes are nonlinear and exhibit interaction effects. Mean annual soil temperature at 90 cm depth is plotted against the normalized snow precipitation, O-horizon macroporosity, water table depth, O-horizon thickness, and air temperature factor values for each model run (blue dots). In each subplot, the red lines link two runs associated by a change in the factor and represent the corresponding change in soil temperature. Factor descriptions and ranges can be found in Table 1.

temperature (Figure 3). The sign of the EE of the O-horizon thickness on 90 cm MAT is linked to the water content of the top 20 cm of soil such that an increase in O-horizon thickness results in an increase in soil temperature in wet soils and a decrease in soil temperatures in dry soils ($R^2 = 0.77$ when there is no associated change in vegetation composition, Figure S5 in Supporting Information S1). The water content of the O-horizon impacts heat transfer to deeper soils by modifying soil thermal properties and latent heat exchanges in the short-term, and PFT competitive dynamics over longer time frames.

The response of soil temperatures to near-surface soil properties that affect water fluxes in the GSA demonstrates that near-surface hydrology is an important control on soil temperature. The magnitude of the offset between MAAT and MAGST created by seasonal snowpack is dependent on heat transfer from the atmosphere to the soil during the summer months, which is strongly affected by the water content of near-surface soils (Sazonova & Romanovsky, 2003; V. E. Romanovsky & Osterkamp, 1995). The presence of macropores in soils (or fractures in bedrock) increases laminar flow and drainage in the model, particularly in organic soils which otherwise have high water retention (Figure S6 in Supporting Information S1). O-horizon macroporosity, which affects the drainage of near-surface soils, has a large mean absolute EE (1.7°C, ranked second of all factors) and a large negative mean EE (−1.5°C) on 90 cm MAT (Figures 2a and 2b). In contrast, the mean absolute EE on 90 cm MAT of A/B-horizon macroporosity, which affects the drainage of deeper soils, is much smaller (0.6°C), and the mean EE is not significant (Figures 2a and 2b). Below the water table, soils will be saturated even if they have large drainage capacity. In these simulations, the external water table factor sets the depth of lateral discharge and recharge of water such that a shallower (deeper) external water table will have wetter (drier) near-surface soils. This factor has a large mean absolute EE (1.6°C) and a large negative mean EE on 90 cm MAT (−1.4°C; Figures 2a and 2b), but the influence of the external water table is highly non-linear. MAT at 90 cm increases if the external water table rises close to the surface, causing more surface wetting and consequently heat transfer, but does not change much for external water tables deeper than 1 m (Figure 3).

Soil water content further influences 90 cm MAT via changes in thermal conductivities associated with freeze-thaw processes. In permafrost systems, increased thermal conductivity and therefore heat transfer in frozen versus unfrozen soils creates a negative offset between MAGST and mean annual soil temperatures (Sazonova & Romanovsky, 2003; V. E. Romanovsky & Osterkamp, 1995). Because of their impact on soil porosity and water influx, drainage, and retention, the O-horizon thickness, O-horizon macroporosity, and external water table depth control changes in soil water and ice content that are responsible for seasonal differences in soil thermal conductivity in *ecosys*. These factors are the most important controls in the GSA on the thermal offset between MAGST and 90 cm MAT (Figures 2a and 2b). Snow also has a strong impact on the modeled thermal offset, even though it is not the dominant control, because it has a strong influence on the ratio of freezing days to thawing days throughout the soil profile.

3.3. Tall Deciduous Shrub Growth Is Associated With Specific Combination of Subsurface Properties

Vegetation composition in *ecosys* is emergent rather than prescribed, and results from competition for light, water, and nutrients. Shrub, moss, and sedge were the most successful PFTs in the GSA, while lichen and grass were never the dominant PFT. We found that the relative success of the shrub, moss, and sedge PFTs are linked to variability in modeled subsurface conditions. In particular, factors that affect soil temperature and water content

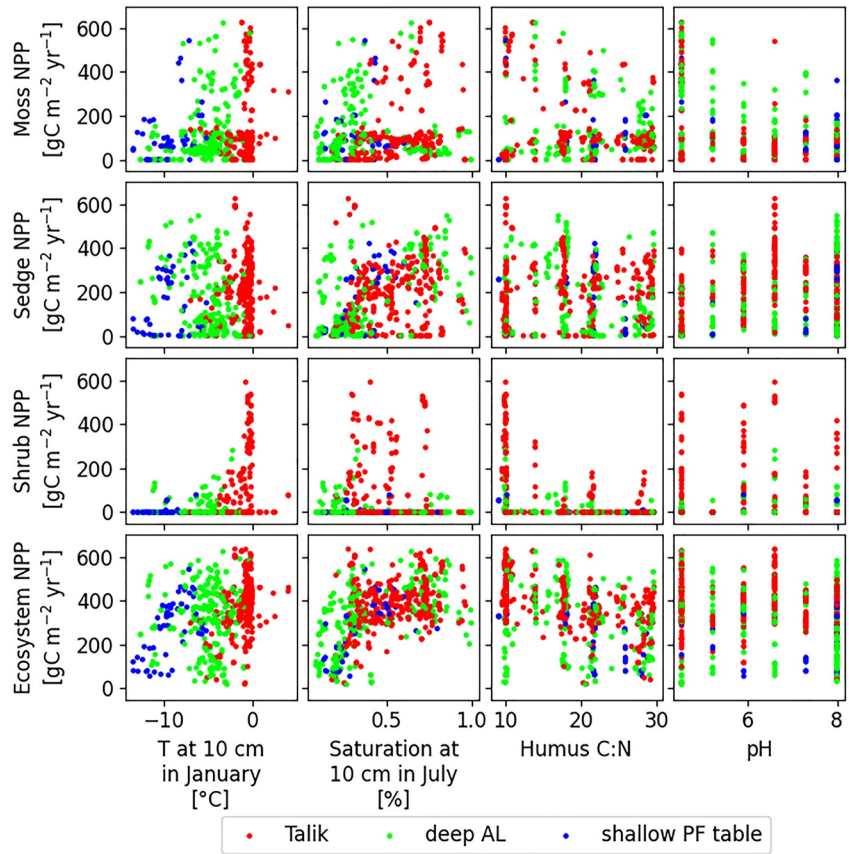

Figure 4. Modeled shrubs are only productive in a specific set of subsurface conditions. Moss, sedge, and shrub NPP for each simulation are plotted against January soil temperature at 10 cm depth, July soil saturation at 10 cm depth, humus C:N, and pH. Each simulation is classified into Talik (red), deep AL (green), or shallow PF table (blue) based on soil temperatures at 90 cm depth.

(OH MP, WT, OH thickness, Air T), nitrogen availability (C:N, OH OM, A/B OM), and pH have large impacts on PFT competition (Figures 2e and 2f).

Whereas moss and sedge PFTs are productive over a large range of conditions, the shrub PFT is sensitive to thermal and hydrological controls on nitrogen uptake and grows only in a specific combination of subsurface conditions (Figure 4). In particular, tall deciduous shrubs grow almost exclusively in simulations with talik, near-surface winter temperatures warmer than −1°C, summertime near-surface water content between 30% and 75% of soil porosity, and low humus C:N ratios (10–15). In these simulations, humus C:N ratios are a strong control on soil nitrogen availability. Since minimum C:N ratios of microbial biomass are fixed in the model, microbial decomposition in nutrient rich soils leads to net mineralization and increased plant nutrient availability (Grant et al., 2010). Additionally, soil water content is an important control on shrub nutrient acquisition, as nutrient mineralization, fixation, and uptake are inhibited by water stress at low soil water contents and by oxygen stress at high soil water contents (Mekonnen, Riley, Grant, et al., 2021). Finally, the association between warm winter soils and shrub productivity is driven by non-growing season nitrogen uptake. Plant community structure and species dominance is shaped by differing nutrient acquisition strategies in high-latitude ecosystems (McKane et al., 2002) and non-growing season nutrient uptake, which occurs at high rates only in Talik runs (Figure S7 in Supporting Information S1), gives a competitive advantage to shrub PFTs at high-latitudes (Riley et al., 2021). We note that non-growing season nutrient dynamics and plant uptake has also been shown to be important for global carbon and nitrogen dynamics (Riley et al., 2018).

3.4. Talik Runs Have Higher Rates of Biological Activity Than Shallow PF Table Runs

The response of ecosystem carbon fluxes to subsurface heterogeneity is complex. In the GSA, R_h and NPP range from near zero to more than 600 gC m^{-2} yr^{-1} (Figure 5). The mean absolute EEs of many of the factors in the

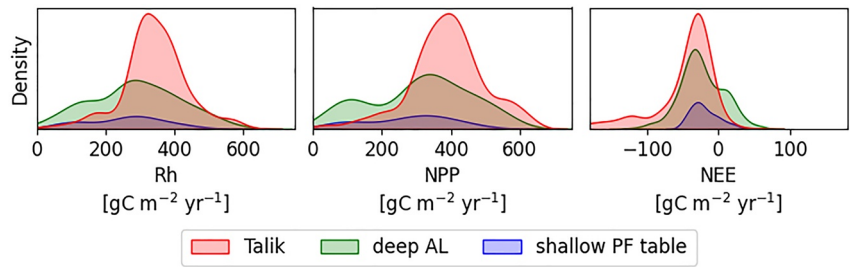

Figure 5. Distributions of carbon fluxes for groups classified by soil temperature at 90 cm depth are distinct. Kernel density estimates of distributions of microbial respiration (R_h), NPP, and NEE (negative values correspond to carbon uptake) are shown for groups of simulations classified by soil temperatures at 90 cm depth (shallow PF table-blue; Deep AL-green; Talik-red). The distributions share a common normalization, such that the area under all curves for a given flux sums to one.

GSA on R_h and NPP are large. Air temperature is an important control on ecosystem carbon fluxes, but incoming shortwave radiation has a larger mean absolute EE for both R_h and NPP. In addition, there are several factors related to subsurface properties (OH MP, WT, OH thickness, C:N) that have similar or larger mean absolute EEs on R_h and NPP than both air temperature and incoming shortwave radiation (Figures 2c and 2d). In general, many of the factors that are important for soil temperatures are also important for R_h and NPP, although the relative importance of each factor is different for the carbon fluxes than for the soil temperatures.

Due to the complexity of the system, we found that a large range of modeled conditions can reproduce observed soil CO_2 fluxes. At one site, we identified 22 of the GSA simulations that accurately matched the observed soil CO_2 fluxes (Nash-Sutcliffe coefficient >0.93; Figure S8 in Supporting Information S1). We note that these 22 simulations span the range of model factors and emergent soil moisture, temperature, and vegetation cover, highlighting the equifinality inherent in this complex system (Luo et al., 2015; Tang & Zhuang, 2008). This equifinality is likely due to interactions between soil temperature and moisture with other factors such as soil carbon, nitrogen cycling, pH, and incoming shortwave radiation, that are shown in the GSA to have a large impact on vegetation dynamics and carbon fluxes (Figures 2c–2f).

Although system complexity creates large variability in modeled R_h and NPP, soil thermal state is an important driver of carbon flux heterogeneity in the GSA. In particular, R_h (NPP) is 78.0 gC m^{-2} yr^{-1} (104.9 gC m^{-2} yr^{-1}) higher when drawn from the Talik distribution than when drawn from the shallow PF table distribution according to the Wilcoxon rank sum test (Figure 5, Table S2 in Supporting Information S1). Indeed, the impact of the soil thermal regime on NPP and R_h is larger than the impact of air temperature over the range covered by this GSA. R_h (NPP) is only 55.0 gC m^{-2} yr^{-1} (62.1 gC m^{-2} yr^{-1}) larger in runs with high air temperature (Air T offset >= 0.6°C) than in runs with low air temperature (Air T offset <= −0.6°C; Wilcoxon rank sum test; Table S2 in Supporting Information S1).

3.5. Missing Representation of Subgrid Heterogeneity Introduces Bias in Estimates of Watershed NEE

Plant and microbial activity are tightly coupled through exchanges of carbon and nitrogen, so simulated R_h and NPP generally respond jointly to subsurface heterogeneity. Increased microbial activity leads to increased plant nitrogen uptake ($R^2 = 0.88$; Figure 6b) which supports increased carbon fixation by plants ($R^2 = 0.89$, Figure 6d). Conversely, increased NPP leads to increased labile carbon inputs into the soil ($R^2 = 0.97$; Figure 6c) that drives increased microbial activity, and hence R_h ($R^2 = 0.99$; Figure 6a). Because of this strong coupling between R_h and NPP, NEE has much lower variability across the simulations (Figure 5). NEE for a sample drawn from the Talik distribution is 15.6 gC m^{-2} yr^{-1} more negative than a sample drawn from the shallow PF table distribution (i.e., greater carbon uptake in the Talik simulations; Wilcoxon rank sum test; Table S2 in Supporting Information S1), but this difference is small compared to the differences between the distributions of NPP and R_h discussed above. In fact, this difference may be attributed to the long left tail in the Talik distribution that is not present in the shallow PF table or deep AL distributions. Simulations with NEE more negative than −100 gC m^{-2} yr^{-1} (i.e., higher net ecosystem carbon uptake) were found almost exclusively in Talik simulations. Within the Talik simulations (depth to talik <= 90 cm), there is no clear trend that relates NEE and depth to talik (Figure S9 in Supporting Information S1).

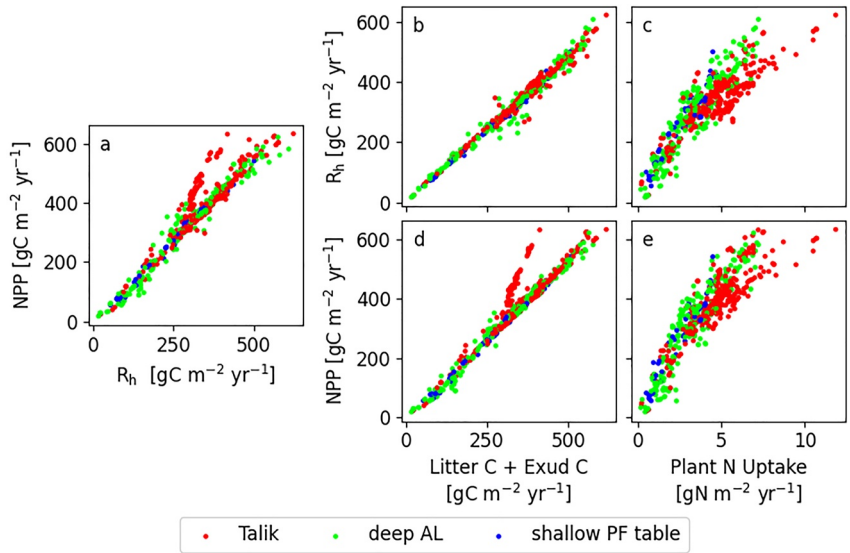

Figure 6. Plant and microbial activity are tightly coupled through exchanges of carbon and nitrogen. Annual R_h and NPP are plotted against annual carbon inputs to the soil (litter carbon + root exudate carbon) and against annual plant nitrogen uptake. Each simulation is classified into Talik (red), deep AL (green), or shallow PF table (blue) based on soil temperatures at 90 cm depth.

Two mechanisms are responsible for breaking the coupling between R_h and NPP in the runs with the highest values of net carbon uptake. First, saturated conditions caused by a shallow water table slow decomposition of plant carbon inputs due to lower energy yields from redox reactions conducted by anaerobic heterotrophic microbial populations, suppressing R_h relative to NPP (Figure 7). Second, allocation to woody structural carbon leads to high carbon retention in tall, productive shrubs (NPP >200 gC m^{-2} yr^{-1}). While moss and sedge PFTs with NPP >200 gC m^{-2} yr^{-1} lose on average 92% and 97% of above- and below-ground carbon fixed each year to litter carbon or root exudates, productive shrubs lose only 66%. Greater carbon retention reduces the percentage of newly fixed and highly labile carbon that is available to microbial decomposition each year, and nearly all of the simulations with productive shrubs have net carbon uptake greater than 100 gC m^{-2} yr^{-1} (Figure 7).

Small scale variation in environmental conditions such as water potentials, soil mineral and organic composition, and nutrient availability are challenging to map across a watershed. However, shifts in plant community composition, which are both an indicator and a driver of landscape heterogeneity, can be identified at high-resolution over large land surface areas due to recent advances in remote sensing (Yang et al., 2021). Patches of tall shrubs, which are associated with the subsurface conditions described in Section 3.3 and outlying values of net carbon uptake, cover 15% of the studied watershed according to a vegetation map (Konduri & Kumar, 2019).

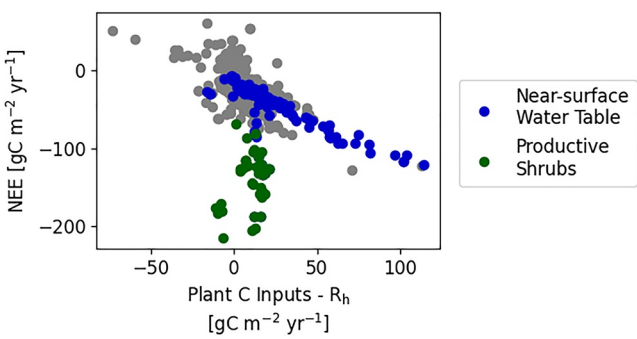

Figure 7. Large net carbon uptake in simulations with near-surface water tables and productive shrubs is achieved via different carbon storage mechanisms for each group. NEE is plotted against the difference between yearly plant C inputs to the soil (litter C and root exudates) and yearly microbial respiration (R_h) for each simulation. Runs with a near-surface water table (depth to external water table = 0.2 m) are shown in blue, runs with productive shrubs (shrub NPP > 200 gC m^{-2} yr^{-1}) are shown in green, and all other runs are shown in gray.

The observed coverage of tall shrub patches can be used to demonstrate that inclusion of landscape heterogeneity can have a large impact on modeled estimates of watershed-scale NEE. We ran a single simulation of the studied watershed using soil data extracted from the Northern Circumpolar Soil Carbon Database (Hugelius et al., 2013) and unmodified weather forcing data. This simulation mimics the setup of a typical large-scale land model used in Earth System Models (e.g., Q. Zhu et al., 2019; Riley et al., 2018). In this simulation, the subsurface conditions are not appropriate for shrub growth, and sedge is the dominant PFT. The mean net carbon uptake for GSA outputs without tall shrubs is 24 gC m^{-2} yr^{-1}. If the shrub patch coverage from the vegetation map is used to weight the GSA outputs, the estimated net carbon uptake for the watershed is 38 gC m^{-2} yr^{-1}. The estimate of watershed net carbon uptake that includes landscape heterogeneity is 60% larger

under current conditions than the estimate of a single model run that does not simulate productive shrub growth. Since high-latitude shrub coverage is projected to expand in the coming decades (Mekonnen et al., 2018), this bias will likely increase rapidly in the short term. We note that if the single model run did simulate productive shrub growth, it would overestimate watershed net carbon uptake through missing representation of the 85% of the watershed not covered by tall shrubs.

3.6. Caveats and Uncertainties

Although our *ecosys* simulations represented many of the important processes for high-latitude carbon cycling, we did not explore here dynamics associated with thermokarst, fire, or herbivory (Mekonnen, Riley, Berner, et al., 2021). Additionally, the simulations were performed using a 1D soil column which is typical of current large-scale land models but may overlook important processes that occur in 3D such lateral flow of heat, water, carbon and nutrients (Jafarov et al., 2018; Mekonnen, Riley, Grant, et al., 2021). Further, our weather forcing perturbations were imposed for the full duration of the simulations (i.e., 183 years), so that short-term dynamics responses to changes were not analyzed, although they can be important (e.g., Bouskill et al., 2020).

There are limitations to scaling up the results of this sensitivity analysis. While we expect that many of the relationships identified by this GSA hold at larger scales, large-scale variations in air temperature, solar radiation, and precipitation will change the response of soil temperatures, vegetation dynamics, and carbon fluxes to each of the factors explored in this GSA. For example, while we expect that the strong influence of snow on soil temperatures and the association between shrub growth and subsurface conditions holds across subarctic tundra ecosystems, we cannot use the results of this GSA to predict soil temperatures or ecosystem carbon fluxes at these larger scales.

4. Conclusions

We show that near-surface hydrology and soil properties drive heterogeneity in soil temperatures, PFT dynamics, and carbon fluxes. We performed a Morris Global Sensitivity Analysis (GSA) of factors related to soil properties, landscape position, and weather forcings. The resulting simulations cover the range of soil temperatures, soil water contents, and soil CO_2 fluxes observed throughout the watershed. In the GSA, snow and factors that affect O-horizon saturation and drainage have a larger impact on soil temperatures than a 2°C variation in MAAT. We split the simulation runs into groups based on soil temperatures at 90 cm depth and found that near-surface talik soils have higher R_h and NPP than near-surface permafrost soils. Because of strong coupling between NPP and R_h, the distribution of NEE is strongly peaked at a value of moderate carbon uptake for near-surface permafrost and near-surface talik runs. The near-surface talik NEE distribution is strongly left skewed, however. Tall productive shrubs grow only when talik is present, January near-surface soil temperatures are warmer than −1°C, summertime near-surface water content is between 30% and 75% of soil porosity, and C:N ratios are lower than 15. Simulations with high shrub productivity decouple R_h from NPP by accumulating carbon in woody material, leading to very high net carbon uptake.

Besides the strong impact of snow on subsurface thermal regimes, organic soils are typically thought to protect permafrost, regardless of water content (Du et al., 2022; Jorgenson et al., 2010). Here, however, we find that the water content of the O-horizon determines whether it will insulate soils. To our knowledge, this finding has not been discussed previously. This result has important implications for ecosystem responses to climate warming at high latitudes. Further investigation is needed to verify this effect in the field, and to determine if it holds only in warm, transitional permafrost environments or if it applies more broadly in the high latitudes.

In arctic tundra ecosystems, patches of tall shrubs are associated with warmer winter soils and increased likelihood for talik formation than surrounding patches of low-lying tundra vegetation (Frost et al., 2018; Myers-Smith & Hik, 2013). This association is attributed to wind-driven accumulation of snow in shrub canopies, implying that talik formation follows shrub growth (Jafarov et al., 2018). In the simulations presented here, however, there is no representation of snow trapping in shrub canopies. Nevertheless, we find that tall shrubs are only productive in talik soils when winter soils are warm enough to permit high rates of nutrient uptake. This result is important because it demonstrates that the association between talik and tall shrubs is driven by biogeochemical processes in addition to the physical snow-trapping mechanism.

Our results indicate that missing representation of landscape heterogeneity in large-scale Earth System Models (which are typically run at resolutions coarser than 50 km) can bias estimates of soil temperatures, vegetation

dynamics, and carbon balance. For example, the success of the shrub PFT in our simulations is strongly dependent on local variability in near-surface hydrological conditions and estimated net carbon uptake for the studied watershed is 60% higher when the measured shrub distribution is accounted for. These results demonstrate the need for better representation of subgrid hydrology and vegetation dynamics in terrestrial ecosystem models, and higher-resolution observations of soil and vegetation properties for model parameterization and validation.

Data Availability Statement

Watershed soil physical and thermal properties used to set factor limits for the GSA can be found at https://doi.org/10.5440/1860505 (Dafflon et al., 2019). Soil temperature and volumetric water content data can be found at https://doi.org/10.5440/1581437 (V. Romanovsky et al., 2020). *Eosense FD* measurements of watershed CO_2 fluxes can be found at https://doi.org/10.5440/1875917 (Shirley, Dafflon, Peterson, et al., 2022). GSA modeling outputs generated for this study can be found at https://doi.org/10.5440/1875918 (Shirley, Dafflon, Mekonnen, et al., 2022).

Acknowledgments
This research was supported by the Director, Office of Science, Office of Biological and Environmental Research of the US Department of Energy under contract no. DE-AC02-05CH11231 to Lawrence Berkeley National Laboratory as part of the Next-Generation Ecosystem Experiments in the Arctic (NGEE-Arctic) project.

References

Arora, B., Wainwright, H. M., Dwivedi, D., Vaughn, L. J. S., Curtis, J. B., Torn, M. S., et al. (2019). Evaluating temporal controls on greenhouse gas (GHG) fluxes in an Arctic tundra environment: An entropy-based approach. *Science of the Total Environment*, *649*, 284–299. https://doi.org/10.1016/j.scitotenv.2018.08.251

Becker, M. S., Jonathan Davies, T., & Pollard, W. H. (2016). Ground ice melt in the high Arctic leads to greater ecological heterogeneity. *Journal of Ecology*, *4*(1), 114–124. https://doi.org/10.1111/1365-2745.12491

Belshe, E. F., Schuur, E. A. G., Bolker, B. M., & Bracho, R. (2012). Incorporating spatial heterogeneity created by permafrost thaw into a landscape carbon estimate. *Journal of Geophysical research: Biogeosciences*, *117*(G1). https://doi.org/10.1029/2011jg001836

Bouskill, N. J., Riley, W. J., Zhu, Q., Mekonnen, Z. A., & Grant, R. F. (2020). Alaskan carbon-climate feedbacks will be weaker than inferred from short-term experiments. *Nature Communications*, *11*(1), 1–12. https://doi.org/10.1038/s41467-020-19574-3

Busey, B., Bolton, B., Wilson, C., & Cohen, L. (2017). Surface meteorology at teller site stations, Seward Peninsula, Alaska, ongoing from 2016 [Dataset]. https://ngee-arctic.ornl.gov/data/pages/NGA079.html

Cable, W. L., Romanovsky, V. E., & Torre Jorgenson, M. (2016). Scaling-up permafrost thermal measurements in Western Alaska using an ecotype approach. *The Cryosphere*. https://doi.org/10.5194/tc-10-2517-2016

Campolongo, F., Cariboni, J., & Saltelli, A. (2007). An effective screening design for sensitivity analysis of large models. *Environmental Modelling & Software*, *22*(10), 1509–1518. https://doi.org/10.1016/j.envsoft.2006.10.004

Dafflon, B., Brunetti, C., Lamb, J., Uhlemann, S., Shirley, I., McClure, P., & Wang, C. (2019). Soil physical and thermal properties from soil samples at multiple locations at Teller Road Site, Seward Peninsula, Alaska, 2019 [Dataset]. ExperimentsArctic. Retrieved from https://ngee-arctic.ornl.gov/data/pages/NGA280.html

Debolskiy, M. V., Nicolsky, D. J., Hock, R., & Romanovsky, V. E. (2020). Modeling present and future permafrost distribution at the Seward Peninsula, Alaska. *Journal of Geophysical research: Earth surface*, *125*(8), e2019JF005355. https://doi.org/10.1029/2019jf005355

Dentener, F. J. (2006). ORNL distributed active archive center datasets. *Global Maps of Atmospheric Nitrogen Deposition*, *1860*, 1993. https://doi.org/10.3334/ornldaac/830

Dimitrov, D. D., Grant, R. F., Lafleur, P. M., & Humphreys, E. R. (2010). Modeling the subsurface hydrology of Mer Bleue Bog. *Soil Science Society of America Journal*, *74*(2). https://doi.org/10.2136/sssaj2009.0148

Du, R., Peng, X., Frauenfeld, O. W., Sun, W., Liang, B., Chen, C., et al. (2022). The role of peat on permafrost thaw based on field observations. *CATENA*, *208*, 105772. https://doi.org/10.1016/j.catena.2021.105772

Farquhar, G. D., von Caemmerer, S., & Berry, J. A. (1980). A biochemical model of photosynthetic CO_2 assimilation in leaves of C_3 species. *Planta*, *149*(1), 78–90. https://doi.org/10.1007/bf00386231

Finger, R. A., Turetsky, M. R., Kielland, K., Ruess, R. W., Mack, M. C., & Euskirchen, E. S. (2016). Effects of permafrost thaw on nitrogen availability and plant–soil interactions in a boreal Alaskan lowland. *Journal of Ecology*, *104*(6), 1542–1554. https://doi.org/10.1111/1365-2745.12639

Frost, G. V., Epstein, H. E., Walker, D. A., Matyshak, G., & Ermokhina, K. (2018). Seasonal and long-term changes to active-layer temperatures after tall Shrubland expansion and succession in Arctic tundra. *Ecosystems*, *21*(3), 507–520. https://doi.org/10.1007/s10021-017-0165-5

Gelaro, R., McCarty, W., Suárez, M. J., Todling, R., Molod, A., Takacs, L., et al. (2017). The Modern-Era Retrospective Analysis for Research and Applications, Version 2 (MERRA-2). *Journal of Climate*, *30*(13), 5419–5454.

Grant, R. F. (1998). Simulation in ecosys of root growth response to contrasting soil water and nitrogen. *Ecological Modelling*, *107*(2–3), 237–264. https://doi.org/10.1016/s0304-3800(97)00221-4

Grant, R. F. (2014). Nitrogen mineralization drives the response of forest productivity to soil warming: Modelling in ecosys versus measurements from the Harvard soil heating experiment. *Ecological Modelling*, *288*, 38–46. https://doi.org/10.1016/j.ecolmodel.2014.05.015

Grant, R. F., Barr, A. G., Black, T. A., Margolis, H. A., Mccaughey, J. H., & Trofymow, J. A. (2010). Net ecosystem productivity of temperate and boreal forests after clearcutting—A fluxnet-Canada measurement and modelling synthesis. *Tellus B: Chemical and Physical Meteorology*, *62*(5), 475–496. https://doi.org/10.1111/j.1600-0889.2010.00500.x

Grant, R. F., & Flanagan, L. B. (2007). Modeling stomatal and nonstomatal effects of water deficits on CO_2 fixation in a semiarid grassland. *Journal of Geophysical research: Biogeosciences*, *112*(G3). https://doi.org/10.1029/2006jg000302

Grant, R. F., Mekonnen, Z. A., & Riley, W. J. (2019). Modeling climate change impacts on an Arctic polygonal tundra: 1. Rates of permafrost thaw depend on changes in vegetation and drainage. *Journal of Geophysical Research: Biogeosciences*, *124*(5), 1308–1322. https://doi.org/10.1029/2018jg004644

Grant, R. F., Mekonnen, Z. A., Riley, W. J., Arora, B., & Torn, M. S. (2017). Mathematical Modelling of Arctic polygonal tundra with ecosys: 2. Microtopography determines how CO_2 and CH_4 exchange responds to changes in temperature and precipitation. *Journal of Geophysical Research: Biogeosciences*, *122*(12), 3174–3187. https://doi.org/10.1002/2017jg004037

Grant, R. F., Mekonnen, Z. A., Riley, W. J., Arora, B., & Torn, M. S. (2019b). Modeling climate change impacts on an arctic polygonal tundra: 2. Changes in CO_2 and CH_4 exchange depend on rates of permafrost thaw as affected by changes in vegetation and drainage. *Journal of Geophysical Research: Biogeosciences*, *124*(5), 1323–1341. https://doi.org/10.1029/2018jg004645

Grant, R. F., Mekonnen, Z. A., Riley, W. J., Wainwright, H. M., Graham, D., & Torn, M. S. (2017). Mathematical Modelling of arctic polygonal tundra with ecosys: 1. Microtopography determines how active layer depths respond to changes in temperature and precipitation. *Journal of Geophysical Research: Biogeosciences*, *122*(12), 3161–3173. https://doi.org/10.1002/2017jg004035

Hugelius, G., Tarnocai, C., Bockheim, J. G., Camill, P., Elberling, B., Grosse, G., et al. (2013). Short communication: A new dataset for estimating organic carbon storage to 3 m depth in soils of the northern circumpolar permafrost region. *Earth System Science Data Discussions*. https://doi.org/10.5194/essdd-6-73-2013

Jafarov, E. E., Coon, E. T., Harp, D. R., Wilson, C. J., Painter, S. L., Atchley, A. L., & Romanovsky, V. E. (2018). Modeling the role of preferential snow accumulation in through talik development and hillslope groundwater flow in a transitional permafrost landscape. *Environmental Research Letters*, *13*(10), 105006. https://doi.org/10.1088/1748-9326/aadd30

Johnson, K. D., Harden, J. W., David McGuire, A., Clark, M., Yuan, F., & Finley, A. O. (2013). Permafrost and organic layer interactions over a climate gradient in a discontinuous permafrost zone. *Environmental Research Letters*. https://doi.org/10.1088/1748-9326/8/3/035028

Jorgenson, M. T., Torre Jorgenson, M., Romanovsky, V., Harden, J., Shur, Y., O'Donnell, J., et al. (2010). Resilience and vulnerability of permafrost to climate change this article is one of a selection of papers from the dynamics of change in Alaska's boreal forests: Resilience and vulnerability in response to climate warming. *Canadian Journal of Forest Research*, *40*(7), 1219–1236. https://doi.org/10.1139/x10-060

Keuper, F., Bodegom, P. M., Dorrepaal, E., Weedon, J. T., Hal, J., Logtestijn, R. S. P., & Aerts, R. (2012). A frozen feast: Thawing permafrost increases plant-available nitrogen in subarctic peatlands. *Global Change Biology*, *18*(6), 1998–2007. https://doi.org/10.1111/j.1365-2486.2012.02663.x

Konduri, S., & Kumar, J. (2019). Hyperspectral remote sensing based vegetation communities around NGEE-Arctic intensive research watersheds at Seward Peninsula, Alaska [Dataset]. https://ngee-arctic.ornl.gov/data/pages/NGA266.html

Lara, M. J., McGuire, A. D., Euskirchen, E. S., Genet, H., Yi, S., Rutter, R., et al. (2020). Local-scale Arctic tundra heterogeneity affects regional-scale carbon dynamics. *Nature Communications*, *11*(1), 4925.

Léger, E., Dafflon, B., Robert, Y., Ulrich, C., Peterson, J. E., Biraud, S. C., et al. (2019). A distributed temperature profiling method for assessing spatial variability in ground temperatures in a discontinuous permafrost region of Alaska. *The Cryosphere*, *13*(11), 2853–2867. https://doi.org/10.5194/tc-13-2853-2019

Luo, Z., Wang, E., Zheng, H., Baldock, J. A., Sun, O. J., & Shao, Q. (2015). Convergent modelling of past soil organic carbon stocks but divergent projections. *Biogeosciences*, *12*(14), 4373–4383. https://doi.org/10.5194/bg-12-4373-2015

McKane, R. B., Johnson, L. C., Shaver, G. R., Nadelhoffer, K. J., Rastetter, E. B., Fry, B., et al. (2002). Resource-based niches provide a basis for plant species diversity and dominance in arctic tundra. *Nature*, *415*(6867), 68–71.

Mekonnen, Z. A., Riley, W. J., Berner, L. T., Bouskill, N. J., Torn, M. S., Iwahana, G., et al. (2021). Arctic tundra shrubification: A review of mechanisms and impacts on ecosystem carbon balance. *Environmental Research Letters*, *16*(5), 053001. https://doi.org/10.1088/1748-9326/abf28b

Mekonnen, Z. A., Riley, W. J., & Grant, R. F. (2018). Accelerated nutrient cycling and increased light competition will lead to 21st century shrub expansion in north American arctic tundra. *Journal of Geophysical Research: Biogeosciences*, *123*(5), 1683–1701. https://doi.org/10.1029/2017jg004319

Mekonnen, Z. A., Riley, W. J., Grant, R. F., Salmon, V. G., Iversen, C. M., Biraud, S. C., et al. (2021). Topographical controls on hillslope-scale hydrology drive shrub distributions on the Seward Peninsula, Alaska. *Journal of Geophysical Research: Biogeosciences*, *126*(2), e2020JG005823. https://doi.org/10.1029/2020jg005823

Mekonnen, Z. A., Riley, W. J., Randerson, J. T., Grant, R. F., & Rogers, B. M. (2019). Expansion of high-latitude deciduous forests driven by interactions between climate warming and fire. *Nature Plants*, *5*(9), 952–958. https://doi.org/10.1038/s41477-019-0495-8

Mekonnen, Z. A., Riley, W. J., Randerson, J. T., Grant, R. F., & Rogers, B. M. (2019b). Expansion of high-latitude deciduous forests driven by interactions between climate warming and fire. *Nature Plants*, *5*(9), 952–958. https://doi.org/10.1038/s41477-019-0495-8

Mezbahuddin, M., Grant, R. F., & Flanagan, L. B. (2016). Modeling hydrological controls on variations in peat water content, water table depth, and surface energy exchange of a boreal Western Canadian fen peatland. *Journal of Geophysical Research: Biogeosciences*, *121*(8), 2216–2242. https://doi.org/10.1002/2016jg003501

Morris, M. D. (1991). Factorial sampling plans for preliminary computational experiments. *Technometrics*, *33*(2), 161–174. https://doi.org/10.1080/00401706.1991.10484804

Myers-Smith, I. H., & Hik, D. S. (2013). Shrub canopies influence soil temperatures but not nutrient dynamics: An experimental test of tundra snow-shrub interactions. *Ecology and Evolution*, *3*(11), 3683–3700. https://doi.org/10.1002/ece3.710

Nobrega, S., & Grogan, P. (2008). Landscape and ecosystem-level controls on net carbon dioxide exchange along a natural Moisture gradient in Canadian low arctic tundra. *Ecosystems*, *11*(3), 377–396. https://doi.org/10.1007/s10021-008-9128-1

O'Neill, H. B., & Burn, C. R. (2017). Talik formation at a snow fence in continuous permafrost, Western Arctic Canada. *Permafrost and periglacial processes*, *28*(3), 558–565. https://doi.org/10.1002/ppp.1905

Park, H., Launiainen, S., Konstantinov, P. Y., Iijima, Y., & Fedorov, A. N. (2018). Modeling the effect of Moss cover on soil temperature and carbon fluxes at a tundra site in northeastern Siberia. *Journal of Geophysical research: Biogeosciences*, *123*(9), 3028–3044. https://doi.org/10.1029/2018jg004491

Riley, W. J., Mekonnen, Z. A., Tang, J., Zhu, Q., Bouskill, N. J., & Grant, R. F. (2021). Non-growing season plant nutrient uptake controls Arctic tundra vegetation composition under future climate. *Environmental Research Letters*, *16*(7), 074047. https://doi.org/10.1088/1748-9326/ac0e63

Riley, W. J., Zhu, Q., & Tang, J. Y. (2018). Weaker land–climate feedbacks from nutrient uptake during photosynthesis-inactive periods. *Nature Climate Change*, *8*(11), 1002–1006. https://doi.org/10.1038/s41558-018-0325-4

Rogelj, J., Forster, P. M., Kriegler, E., Smith, C. J., & Séférian, R. (2019). Estimating and tracking the remaining carbon budget for stringent climate targets. *Nature*, *571*(7765), 335–342. https://doi.org/10.1038/s41586-019-1368-z

Romanovsky, V., Cable, W., & Kirill, D. (2020). Soil temperature and Moisture, teller road Mile marker 27, Seward Peninsula, Alaska, beginning 2016 [Dataset]. Retrieved from https://www.osti.gov/dataexplorer/biblio/dataset/1581437

Romanovsky, V. E., & Osterkamp, T. E. (1995). Interannual variations of the thermal regime of the active layer and near-surface permafrost in northern Alaska. *Permafrost and Periglacial Processes*, *6*(4), 313–335. https://doi.org/10.1002/ppp.3430060404

Ruano, M. V., Ribes, J., Seco, A., & Ferrer, J. (2012). An improved sampling strategy based on trajectory design for application of the Morris method to systems with many input factors. *Environmental Modelling & Software*, *37*, 103–109. https://doi.org/10.1016/j.envsoft.2012.03.008

Sazonova, T. S., & Romanovsky, V. E. (2003). A model for regional-scale estimation of temporal and spatial variability of active layer thickness and mean annual ground temperatures. *Permafrost and Periglacial Processes*, *14*(2), 125–139. https://doi.org/10.1002/ppp.449

Schuur, E. A. G., McGuire, A. D., Schädel, C., Grosse, G., Harden, J. W., Hayes, D. J., et al. (2015). Climate change and the permafrost carbon feedback. *Nature*. https://doi.org/10.1038/nature14338

Shirley, I. A., Dafflon, B., Mekonnen, Z., Riley, W. J., & Grant, R. (2022). Near-surface hydrology and soil properties drive heterogeneity in permafrost distribution, vegetation dynamics, and carbon cycling in a sub-arctic watershed: Modeling archive [Data set]. https://ngee-arctic.ornl.gov/data/pages/NGA286.html

Shirley, I. A., Dafflon, B., Peterson, J., & Uhlemann, S. (2022). Forced diffusion chamber Monitoring of soil CO2 fluxes from 2019 to present at NGEE arctic teller site, Mile marker 27 [Dataset]. Alaska. https://ngee-arctic.ornl.gov/data/pages/NGA285.html

Shirley, I. A., Mekonnen, Z. A., Grant, R. F., Dafflon, B., Hubbard, S. S., & Riley, W. J. (2022). Rapidly changing high-latitude seasonality: Implications for the 21st century carbon cycle in Alaska. *Environmental Research Letters*, *17*(1), 014032. https://doi.org/10.1088/1748-9326/ac4362

Slivinski, L. C., Compo, G. P., Sardeshmukh, P. D., Whitaker, J. S., McColl, C., Allan, R. J., et al. (2021). An evaluation of the performance of the twentieth century Reanalysis version 3. *Journal of Climate*, *34*(4), 1417–1438. https://doi.org/10.1175/jcli-d-20-0505.1

Strandberg, G., & Lind, P. (2021). The importance of horizontal model resolution on simulated precipitation in Europe—From global to regional models. *Weather and Climate Dynamics*, *2*(1), 181–204. https://doi.org/10.5194/wcd-2-181-2021

Tang, J., & Zhuang, Q. (2008). Equifinality in parameterization of process-based biogeochemistry models: A significant uncertainty source to the estimation of regional carbon dynamics. *Journal of Geophysical research: Biogeosciences*, *113*(G4). https://doi.org/10.1029/2008jg000757

Taras, B., Sturm, M., & Liston, G. E. (2002a). Snow–ground interface temperatures in the Kuparuk River Basin, Arctic Alaska: Measurements and Model. *Journal of Hydrometeorology*, *3*(4), 377–394.

Taras, B., Sturm, M., & Liston, G. E. (2002b). Snow–ground interface temperatures in the Kuparuk River Basin, Arctic Alaska: Measurements and Model. *Journal of hydrometeorology*, *3*(4), 377–394. https://doi.org/10.1175/1525-7541(2002)003

Treat, C. C., Marushchak, M. E., Voigt, C., Zhang, Y., Tan, Z., Zhuang, Q., et al. (2018). Tundra landscape heterogeneity, not interannual variability, controls the decadal regional carbon balance in the Western Russian Arctic. *Global Change Biology*, *24*(11), 5188–5204. https://doi.org/10.1111/gcb.14421

Uhlemann, S., Dafflon, B., Peterson, J., Ulrich, C., Shirley, I., Michail, S., & Hubbard, S. S. (2021). Geophysical Monitoring shows that spatial heterogeneity in thermohydrological dynamics reshapes a transitional permafrost system. *48*(6), e2020GL091149. *Geophysical Research Letters*. https://doi.org/10.1029/2020gl091149

Wainwright, H. M., Finsterle, S., Jung, Y., Zhou, Q., & Birkholzer, J. T. (2014). Making sense of global sensitivity analyses. *Computers & Geosciences*, *65*, 84–94. https://doi.org/10.1016/j.cageo.2013.06.006

Waldrop, M. P., McFarland, J., Manies, K. L., Leewis, M. C., Blazewicz, S. J., Jones, M. C., et al. (2021). Carbon fluxes and Microbial activities from boreal peatlands experiencing permafrost thaw. *Journal of Geophysical Research: Biogeosciences*, *126*(3), e2020JG005869. https://doi.org/10.1029/2020jg005869

Wei, Y., Liu, S., Huntzinger, D. N., Michalak, A. M., Viovy, N., Post, W. M., et al. (2014). The North American carbon program Multi-scale synthesis and terrestrial Model Intercomparison project—Part 2: Environmental driver data. *Geoscientific Model Development*, *7*(6), 2875–2893.

Wu, Y., Ulrich, C., Kneafsey, T., Lopez, R., Chou, C., Geller, J., et al. (2018). Depth-resolved physicochemical characteristics of active layer and permafrost soils in an Arctic polygonal tundra region. *Journal of Geophysical Research: Biogeosciences*, *123*(4), 1366–1386. https://doi.org/10.1002/2018jg004413

Yang, D., Morrison, B. D., Hantson, W., Breen, A. L., McMahon, A., Li, Q., et al. (2021). Landscape-scale characterization of Arctic tundra vegetation composition, structure, and function with a multi-sensor unoccupied aerial system. *Environmental Research Letters*, *16*(8), 085005. https://doi.org/10.1088/1748-9326/ac1291

Zhu, D., Ciais, P., Krinner, G., Maignan, F., Jornet Puig, A., & Hugelius, G. (2019). Controls of soil organic matter on soil thermal dynamics in the northern high latitudes. *Nature Communications*, *10*(1), 1–9. https://doi.org/10.1038/s41467-019-11103-1

Zhu, Q., Riley, W. J., Tang, J., Collier, N., Hoffman, F. M., Yang, X., & Bisht, G. (2019). Representing Nitrogen, Phosphorus, and Carbon Interactions in the E3SM Land Model: Development and Global Benchmarking. *Journal of Advances in Modeling Earth Systems*, *11*, (7), 2238–2258. https://doi.org/10.1029/2018ms001571

Zoltai, S. C. (1993). Cyclic development of permafrost in the peatlands of northwestern Alberta, Canada. *Arctic and Alpine Research*. https://doi.org/10.2307/1551820